Xianlin Zheng, Xingjun Zhu, Yiqing Lu, Jiangbo Zhao, Wei Feng, Guohua Jia, Fan Wang, Fuyou Li, and Dayong Jin

High-contrast visualization of upconversion luminescence in mice using time-gating approach

Analytical Chemistry, 2016; 88(7):3449-3454

analytical chemistry

Technical Note

pubs.acs.org/ac

High-Contrast Visualization of Upconversion Luminescence in Mice Using Time-Gating Approach

Xianlin Zheng,[†] Xingjun Zhu,[‡] Yiqing Lu,[†] Jiangbo Zhao,[†,§] Wei Feng,[‡] Guohua Jia,[∥,⊥] Fan Wang,[†,⊥] Fuyou Li,[*,‡] and Dayong Jin[*,†,⊥]

[†]Advanced Cytometry Laboratories, ARC Centre of Excellence for Nanoscale BioPhotonics (CNBP), Macquarie University, Sydney, New South Wales 2109, Australia

[‡]Department of Chemistry & Institutes of Biomedical Sciences & State Key Laboratory of Molecular Engineering of Polymers, Fudan University, Shanghai, 200433, PR China

[§]Institute for Photonics and Advanced Sensing and School of Physical Sciences, University of Adelaide, Adelaide, South Australia 5005, Australia

[∥]Nanochemistry Research Institute, Department of Chemistry, Curtin University, Perth, Western Australia 6102, Australia

[⊥]Institute for Biomedical Materials and Devices, Faculty of Science, University of Technology Sydney, Sydney, New South Wales 2007, Australia

Supporting Information

ABSTRACT: Optical imaging through the near-infrared (NIR) window provides deep penetration of light up to several centimeters into biological tissues. Capable of emitting 800 nm luminescence under 980 nm illumination, the recently developed upconversion nanoparticles (UCNPs) suggest a promising optical contrast agent for *in vivo* bioimaging. However, presently they require high-power lasers to excite when applied to small animals, leading to significant scattering background that limits the detection sensitivity as well as a detrimental thermal effect. In this work, we show that the time-gating approach implementing pulsed illumination from a NIR diode laser and time-delayed imaging synchronized via an optical chopper offers detection sensitivity more than 1 order of magnitude higher than the conventional approach using optical band-pass filters (S/N, 47321/6353 vs 5339/58), when imaging UNCPs injected into Kunming mice. The pulsed laser illumination (70 μs ON in 200 μs period) also reduces the overall thermal accumulation to 35% of that under the continuous-wave mode. Technical details are given on setting up the time-gating unit comprising an optical chopper, a pinhole, and a microscopy eyepiece. Being generally compatible with any camera, this provides a convenient and low cost solution to NIR animal imaging using UCNPs as well as other luminescent probes.

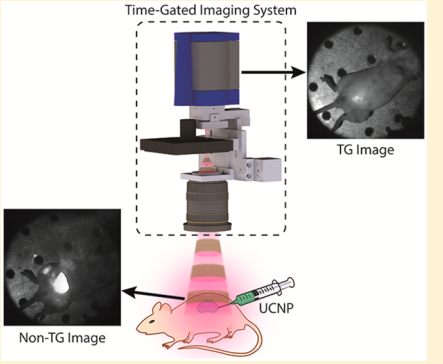

Near-infrared (NIR) optical imaging has drawn increasing attention due to the desire for whole animal and deep tissue imaging at high resolution.[1,2] This is because (1) NIR light of 700−1100 nm is capable of penetrating several centimeters into tissues with much lower scattering compared to visible wavelengths[3−5] and (2) much lower autofluorescence background exists in the NIR range, facilitating sensitive fluorescence detection.[6,7] Thanks to the availability of NIR fluorescent dyes such as indocyanine green, *in vivo* NIR imaging has been adopted preclinically and clinically for identifying disease biomarkers,[8,9] monitoring disease progression,[10,11] determining the pharmaceutical effects of new drugs,[12−14] and fluorescence image-guided surgery.[15−17] Other nanoprobes, such as dye-encapsulated silica nanoparticles and semiconductor quantum dots, have also been proposed and demonstrated for quality NIR imaging under preclinical settings.[18−22]

Compared to these down-conversion materials, lanthanide-based upconversion nanoparticles (UCNPs) offers a promising alternative with their unique anti-Stokes-shifted and long-lived luminescence.[23−25] The past decade has witnessed rapid progress in material science to develop highly controlled UCNPs as a new type of high-sensitive, photostable, low-toxic, and multifunctional optical contrast agent for broad biological and biomedical applications.[26−31] In particular, UCNPs codoped with Yb^{3+} and Tm^{3+} ions are capable of stepwise absorbing 980 nm low-energy photons and emitting strong 800 nm luminescence, thus suitable for deep-tissue imaging in the NIR window.[14,32−39] However, when whole animals are interrogated in practice, substantial scattering from skin and fur is often encountered for the excitation light as well as the emission luminescence, dramatically reducing the imaging contrast and blurring the targeted area.[4,40,41] Additionally, high excitation power under the continuous-wave mode is

Received: December 6, 2015
Accepted: February 25, 2016

DOI: 10.1021/acs.analchem.5b04626
Anal. Chem. XXXX, XXX, XXX−XXX

typically used, resulting in accumulated absorption and thermal effect that adversely affects or even damages the samples.[42]

To overcome these challenges, one opportunity arises from the long luminescence lifetimes of UCNPs (tens to hundreds of microseconds) that allows the time-gated luminescence (TGL) technique to be applied. We have previously demonstrated TGL microscopes employing pulsed excitation and time-delayed detection to eliminate short-lived background from autofluorescence (with lifetimes typically of ∼nanoseconds), achieving high detection sensitivity and imaging contrast using long-lived luminescent probes.[43−45] In this paper, we explore the time-gating approach for NIR imaging of UCNPs in small animals. We demonstrate a system consisting of a fast-switchable 980 nm diode laser and a high-speed optical chopper, which is precisely synchronized for high-contrast time-gated imaging without posing any restrictions on the camera. The performance is evaluated in comparison to the conventional filter-based imaging approach, using Kunming mice injected with water-soluble Yb^{3+}/Tm^{3+} codoped UCNPs as the model.

EXPERIMENTAL SECTION

TGL Imaging System. The schematic diagram of the TGL system for *in vivo* animal imaging is given in Figure 1. Briefly, a time-gating unit comprising a high-speed optical chopper and a microscope eyepiece (Olympus WHN10X) was inserted between a camera lens (Nikon SIGMA 50MM F1.4 EX DG HSM) and an EMCCD camera (Andor iXon Ultra 897). TGL

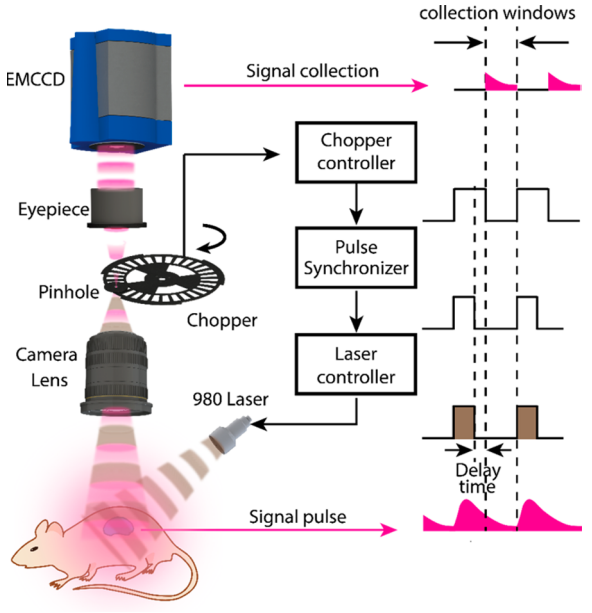

Figure 1. Schematics illustrating the TGL system for *in vivo* NIR imaging. The optical chopper (5 kHz, 1:1 duty ratio) generates a TTL pulse from its reference output to trigger an in-house pulse synchronizer, which times a fixed 70 μs pulse (with 5 μs delay from the chopper output) to enable the 980 nm NIR laser. The pulsed 980 nm light illuminates the mouse to excite the UCNPs. The luminescence signal is collected by a camera lens, passes through a 1 mm pinhole attached to the optical chopper, relayed by a microscope eyepiece, and recorded by an EMCCD camera for *in vivo* imaging. The delay time between the switching-off of the 980 nm pulse and the switching-on of the EMCCD via chopping is 25 μs, followed by a collection window of 100 μs.

imaging was realized by synchronizing the chopper with a pulsed 980 nm fiber-coupled diode laser (LE-LS-980-10000T FC, LEO Photonics; maximum output power 10 W) in antiphase, so that the detection path only opened after the laser switched off and any short-lived background decayed to negligible. The chopper used here (C995, Terahertz Technologies) had a blade consisting of 30 slots with a duty cycle of 1:1. When operating at maximum frequency of 5 kHz (with an accuracy of 0.001 Hz), it gave a rotational speed of ∼167 rev/s. A 1 mm diameter pinhole aperture was attached very close to the chopper blade at a radius of 4.2 cm, so that an ON/OFF switching time of 23 μs was achieved for the signal light and any stray light was removed. The chopper output a TTL signal, generated from the slotted optical switch built in the chopper head, to trigger a homemade pulse synchronizer. The latter delivered pulses of 70 μs duration to the laser controller/driver to switch on the 980 nm laser when the detection path was blocked by the chopper blade, so that the EMCCD camera became effectively time-gated. Delay times of 5 μs and 25 μs were applied before and after the laser pulses, respectively, for optimizing the time-gating performance in practice.

***In Vivo* Animal Imaging.** Hydrophilic $NaLuF_4$:Yb,Tm UCNPs were injected hypodermically in the abdomen of Kunming mice (refer to Supporting Information S1 for details). Under the imaging system, they were illuminated with the pulsed 980 nm laser beam output from the fiber without collimation, at an average intensity of 3.18 W/cm^2. The luminescence signal from the UCNPs was collected by the camera lens, purified by the time-gating unit, and recorded by the EMCCD camera. For comparison, the same mice were also imaged using the conventional filter-based approach under continuous-wave 980 nm excitation at the identical intensity, and the upconversion luminescence was collected with one or two pieces of band-pass filters (FF01-800/12, Semrock) inserted in the detection path while the optical chopper was switched off. Bright-field imaging was also conducted simultaneously alongside the time-gated imaging, using a compact light-emitting diode (LED) to illuminate the mice.

Thermal Effect Evaluation. Thermal images and temperature elevation curves of mice under continuous-wave and time-gated 980 nm laser were recorded by an infrared thermal camera (FLIR E40). As a typical procedure, mice were anesthetized first through intraperitoneal injection of ketamine/xylazine solution (75 mg kg^{-1} ketamine and 15 mg kg^{-1} xylazine) and then placed under the in vivo imaging system. The thermal camera recorded the temperature changes of mice when the 980 nm laser was switched on and irradiated the mice for half a minute. After the recording, the laser was switched off and the mice were placed on warming pad to avoid an excessive body temperature decrease. Temperature elevation curves were produced using the maximum temperature value in the irradiated region versus irradiation time.

RESULTS AND DISCUSSION

We compared the imaging contrast obtained by our time-gating approach with that using the conventional filter-based, nontime-gating approach. Although the band-pass filter used here should have eliminated residual excitation at 980 nm as well as other optical background, so that the camera only collected NIR emission within the range of 800 ± 6 nm (Figure 2a), in reality strong signal was also observed from the surroundings of the injection site (Figure 2b). Along a line drawn across the injection area on the 16-bit grayscale image,

DOI: 10.1021/acs.analchem.5b04626
Anal. Chem. XXXX, XXX, XXX−XXX

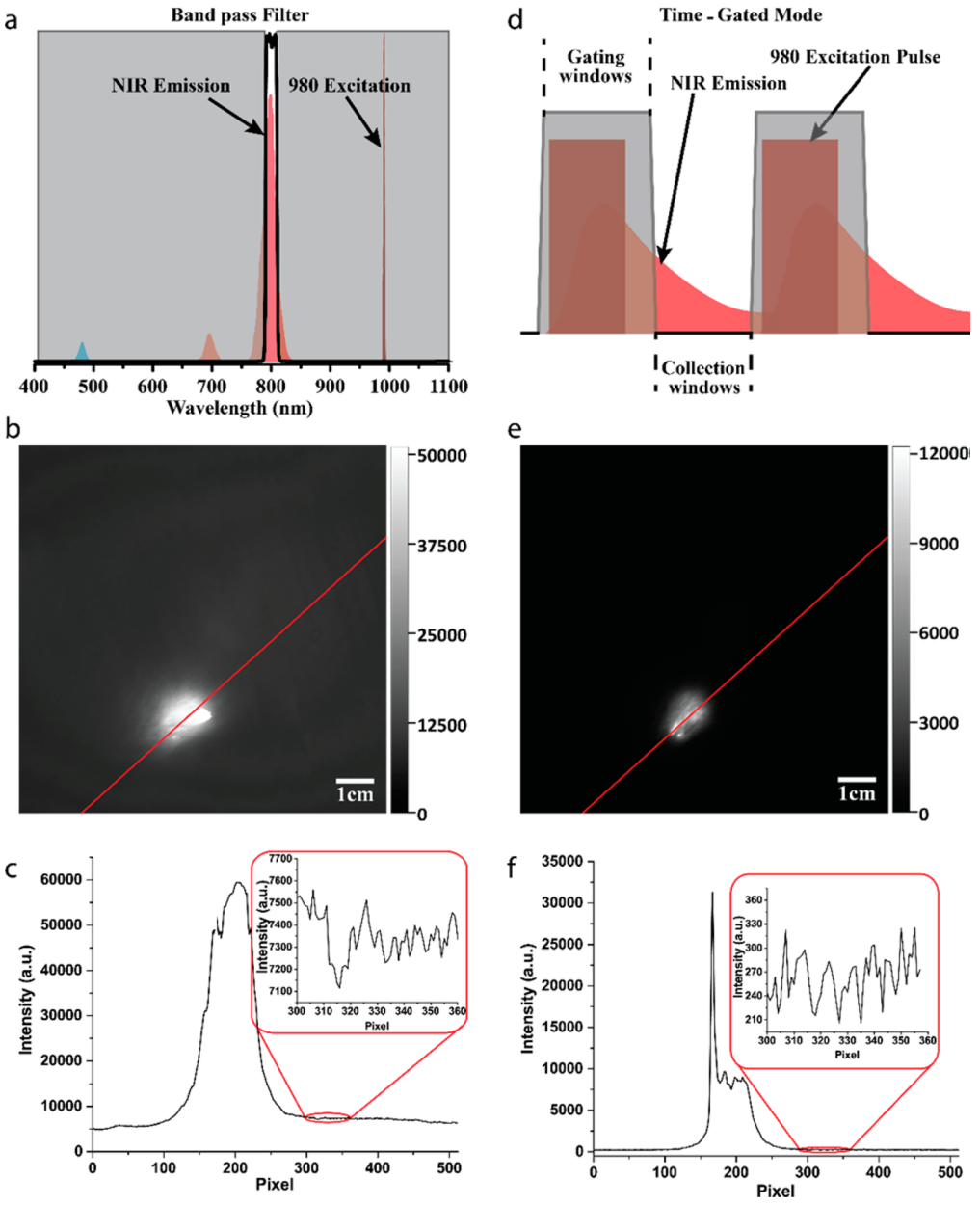

Figure 2. Comparison of *in vivo* imaging contrast between the filter-based approach and the time-gating approach. (a) Spectra of the excitation source, the UCNP luminescence, and the transmission of the band-pass filter. (b) The luminescence image of a Kunming mouse with subcutaneous injection of hydrophilic $NaLuF_4$:Yb,Tm UCNPs (200 μL, 1 mg/mL), obtained by the filter-based approach under CW 980 nm excitation. (c) The intensity profile along the line across the 16-bit grayscale image in part b. (d) The temporal configuration for time-gated imaging. (e) The time-gated image of the same Kunming mouse. (f) The intensity profile along the line across the 16-bit grayscale image in part e. The highest peak corresponds to the actual injection position. The images in parts b and e were captured by the EMCCD camera with an exposure time of 0.4 s and gain of 10, under an average 980 nm excitation intensity of 3.18 W/cm^2 measured on the object mouse. Note that the EMCCD camera was not saturated during the image acquisition.

the maximum intensity recorded was 59 470; nevertheless, the average intensity in the background area also reached 7309 yielding a signal-to-noise ratio of merely 8.13 (Figure 3c). By contrast, the time-gating approach employed pulsed excitation of identical peak intensity but 35% duration and gated detection of 50% duty ratio with the same camera settings (Figure 2d). The image, shown as Figure 2e, was taken immediately after Figure 2b was captured to ensure fair comparison, and a well-defined injection site was revealed against the background area. Along the same line drawn across, although the average intensity in the injection site decreased to 8160 (the outstanding peak intensity, 31 314, corresponds to the actual injection position) due to the effectively reduced excitation and detection time, that of the background area was suppressed more substantially down to 263, so that an enhanced signal-to-noise ratio of 31 was achieved (Figure 2f). Further analysis over the entire images showed the overall signal-to-noise ratio was improved by 12.4-fold using the time-gating approach over the nontime-gated approach (see Supporting Information S2 and Supporting Table 1).

The high optical background here associated with the conventional approach arose from the strong scattering of the

DOI: 10.1021/acs.analchem.5b04626
Anal. Chem. XXXX, XXX, XXX−XXX

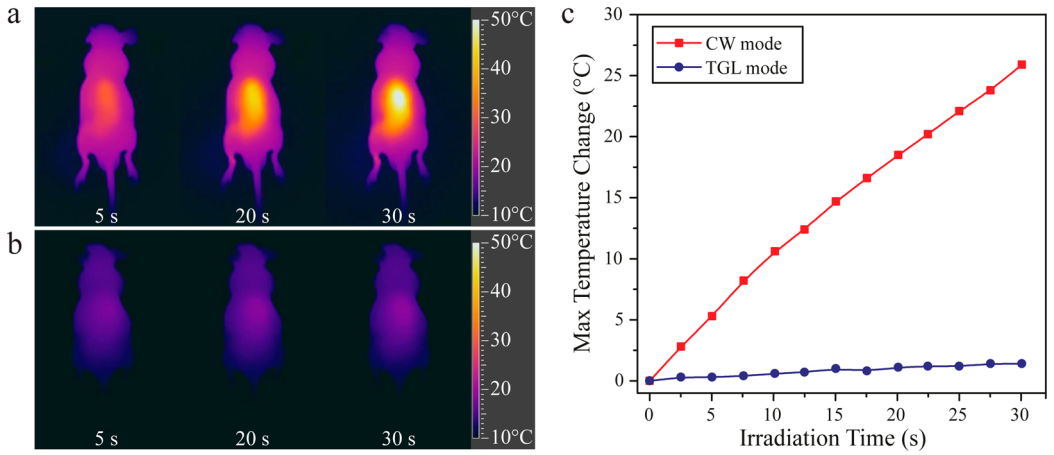

Figure 3. Comparison of the thermal effect between the CW mode and the TGL mode. (a) The thermal images of a Kunming mouse under CW 980 nm laser illumination for 5, 20, and 30 s. (b) The thermal images of a Kunming mouse under pulsed 980 nm laser illumination employed in the TGL mode for 5, 20, and 30 s. (c) The maximum temperature elevation over the irradiated area as a function of irradiation time under the CW and TGL modes.

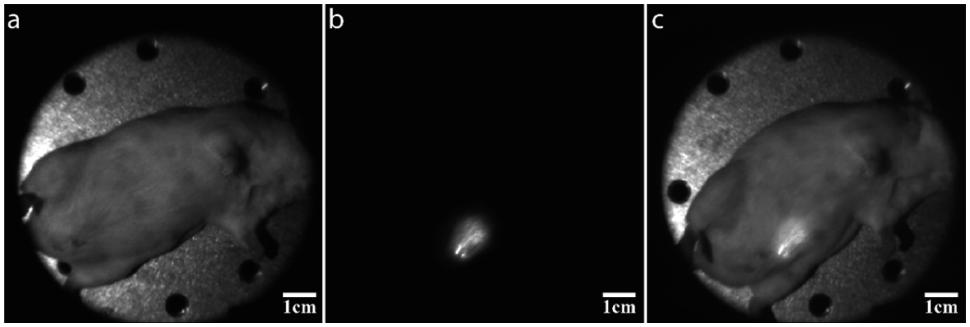

Figure 4. Dual-modal *in vivo* animal imaging. (a) A bright-field image of a Kunming mouse with subcutaneous injection of hydrophilic $NaLuF_4$:Yb,Tm UCNPs (200 μL, 1 mg/mL) under a white LED illumination. (b, c) The time-gated luminescence image of the same Kunming mouse in (a) under 980 nm excitation in the absence (b) and presence (c) of the bright-field LED illumination. All images were taken by the EMCCD camera with exposure time of 0.4 s and gain of 10. The average 980 nm excitation intensity was 3.18 W/cm^2 measured on the object mouse.

excitation light from the animal that one optical filter failed to block. It could be improved by adding more filters, but the effect was still inferior to the time-gating approach (see Supporting Information S3). One possible reason for that was the scattering light had a variety of incident angles, which may also change depending on the position of the animal, making it difficult for the interference-type filters to suppress completely due to their angle-dependent transmission/reflection spectra. Substitution for absorption-type (color-glass) filters is also not possible, as no suitable candidate is currently available to separate 808 nm emission from 980 nm excitation for the UCNPs used here. Moreover, in the conventional approach the background may increase further for animals with colored skin and/or fur that introduce pigmentation-related NIR autofluorescence.[41] Nevertheless, the time-gating approach effectively removed residual scattering of the excitation light as well as autofluorescence regardless of it spectrum or incident angle, so that the background was limited close to the electronic noise level of the camera. On the other hand, while the excitation intensity remained identical, the exposure duration to the excitation light was reduced to 35% (70 μs ON-time in every 200 μs period) under the time-gated mode. This reduced the thermal effect to the animals very effectively. As shown in Figure 3, the maximum temperature increased over 25 °C on the mouse in only 30 s under the CW laser irradiation (same conditions as used in the luminescence imaging), while the temperature change remained negligible for the time-gated mode.

The high signal-to-noise ratio without spectral filtering further allows the time-gated approach to be implemented alongside bright-field visualization, which was demonstrated using the same mice model. As shown in Figure 4, after adjusting the relative brightness of the white LED light with reference to the 980 nm laser excitation to ensure similar levels of intensity were obtained for the respective bright-field and time-gated luminescence images (Figure 4a,b), the time-gated imaging was directly performed in the presence of the LED light to visualize both the entire animal and the UCNP injection site in real time (Figure 4c). This capability, which is not suitable using the conventional approach (see Supporting Information S4), offers significant potential for practical applications, such as luminescence image-guided surgery.

CONCLUSIONS

We have realized time-gated luminescence imaging of upconversion nanoparticles upon live small animals. In contrast to the conventional filter-based approach that suffers from the strong scattering of the excitation light, the time-gating approach is capable of efficient elimination of such background, allowing us to achieve a 12-fold enhancement in the signal-to-

DOI: 10.1021/acs.analchem.5b04626
Anal. Chem. XXXX, XXX, XXX−XXX

noise ratio using Kunming mice injected with UCNPs as the *in vivo* animal model. The overall exposure was reduced to 35%, alleviating overheating as well as other side effects associated with the NIR excitation light. Apart from the Yb/Tm codoped UCNPs, the technique is applicable to other long-lived luminescent probes with lifetimes in the microsecond-to-millisecond region.[46] For example, the Nd-sensitized UCNPs that are excitable at 800 nm[47−49] can be used to further improve the temperature control as well as tissue penetration depth. Furthermore, the time-gated luminescence imaging can be conducted directly under bright-field visualization. These advancements alongside the low cost of our well-engineered instrumentation address the key issues to implement upconversion nanoparticles for deep-tissue NIR imaging in practice, paving the way for their use in biomedical diagnostics as well as multifunctional applications.

■ ASSOCIATED CONTENT

Supporting Information

The Supporting Information is available free of charge on the ACS Publications website at DOI: 10.1021/acs.analchem.5b04626.

Sample preparation, TEM image of oleate NaLuF4:Yb,Tm UCNPs, upconversion spectrum of NaLuF4:Yb,Tm UCNPs, evaluation of signal-to-noise ratio; effect on image contrast using multiple filters, and non-time-gated imaging under the both 980 nm excitation and bright-field illumination (PDF)

■ AUTHOR INFORMATION

Corresponding Authors

*E-mail: dayong.jin@uts.edu.au.

*E-mail: fyli@fudan.edu.cn.

Notes

The authors declare no competing financial interest.

■ ACKNOWLEDGMENTS

The authors acknowledge the financial support from the Australian Research Council (Centre of Excellence for Nanoscale BioPhotonics, Future Fellowship of D.J. Grant FT130100517) and Macquarie University (Postgraduate Scholarship of X.Z., Research Fellowship of Y.L.) and assistance in manufacturing the components for the animal imaging system provided by Macquarie Engineering & Technical Services (METS).

■ REFERENCES

(1) Leblond, F.; Davis, S. C.; Valdés, P. A.; Pogue, B. W. *J. Photochem. Photobiol., B* **2010**, *98*, 77−94.

(2) Quek, C.-H.; Leong, K. W. *Nanomaterials* **2012**, *2*, 92−112.

(3) Frangioni, J. V. *Curr. Opin. Chem. Biol.* **2003**, *7*, 626−634.

(4) Cerussi, A. E.; Berger, A. J.; Bevilacqua, F.; Shah, N.; Jakubowski, D.; Butler, J.; Holcombe, R. F.; Tromberg, B. J. *Academic radiology* **2001**, *8*, 211−218.

(5) Pansare, V. J.; Hejazi, S.; Faenza, W. J.; Prud'homme, R. K. *Chem. Mater.* **2012**, *24*, 812−827.

(6) Wagnieres, G. A.; Star, W. M.; Wilson, B. C. *Photochem. Photobiol.* **1998**, *68*, 603−632.

(7) Adams, K. E.; Ke, S.; Kwon, S.; Liang, F.; Fan, Z.; Lu, Y.; Hirschi, K.; Mawad, M. E.; Barry, M. A.; Sevick-Muraca, E. M. *J. Biomed. Opt.* **2007**, *12*, 024017−024019.

(8) Kosaka, N.; Ogawa, M.; Choyke, P. L.; Kobayashi, H. *Future Oncol.* **2009**, *5*, 1501−1511.

(9) Hawrysz, D. J.; Sevick-Muraca, E. M. *Neoplasia* **2000**, *2*, 388−417.

(10) Gurfinkel, M.; Ke, S.; Wen, X.; Li, C.; Sevick-Muraca, E. M. *Dis. Markers* **2004**, *19*, 107−121.

(11) Du, Y.; An, S.; Liu, L.; Li, L.; Zhou, X. J.; Mason, R. P.; Mohan, C. *PLoS One* **2012**, *7*, e43941.

(12) Reich, G. *Adv. Drug Delivery Rev.* **2005**, *57*, 1109−1143.

(13) Roggo, Y.; Jent, N.; Edmond, A.; Chalus, P.; Ulmschneider, M. *Eur. J. Pharm. Biopharm.* **2005**, *61*, 100−110.

(14) Dai, Y.; Xiao, H.; Liu, J.; Yuan, Q.; Ma, P. a.; Yang, D.; Li, C.; Cheng, Z.; Hou, Z.; Yang, P.; Lin, J. *J. Am. Chem. Soc.* **2013**, *135*, 18920−18929.

(15) De Grand, A. M.; Frangioni, J. V. *Technol. Cancer Res. Treat.* **2003**, *2*, 553−562.

(16) Gioux, S.; Choi, H. S.; Frangioni, J. V. *Mol. Imag.* **2010**, *9*, 237.

(17) Hutteman, M.; Mieog, J.; Van der Vorst, J.; Dijkstra, J.; Kuppen, P.; van der Laan, A.; Tanke, H.; Kaijzel, E.; Que, I.; van de Velde, C.; Lowik, C. W. G. M.; Vahrmeijer, A. L. *Eur. J. Surg. Oncol. (EJSO)* **2011**, *37*, 252−257.

(18) Michalet, X.; Pinaud, F.; Bentolila, L.; Tsay, J.; Doose, S.; Li, J.; Sundaresan, G.; Wu, A.; Gambhir, S.; Weiss, S. *Science* **2005**, *307*, 538−544.

(19) Caltagirone, C.; Bettoschi, A.; Garau, A.; Montis, R. *Chem. Soc. Rev.* **2015**, *44*, 4645−4671.

(20) Zhu, Y.; Hong, H.; Xu, Z. P.; Li, Z.; Cai, W. *Curr. Mol. Med.* **2013**, *13*, 1549−1567.

(21) He, X.; Gao, J.; Gambhir, S. S.; Cheng, Z. *Trends Mol. Med.* **2010**, *16*, 574−583.

(22) Kim, S.; Lim, Y. T.; Soltesz, E. G.; De Grand, A. M.; Lee, J.; Nakayama, A.; Parker, J. A.; Mihaljevic, T.; Laurence, R. G.; Dor, D. M. *Nat. Biotechnol.* **2004**, *22*, 93−97.

(23) Wang, F.; Liu, X. *Chem. Soc. Rev.* **2009**, *38*, 976−989.

(24) Zhao, J.; Jin, D.; Schartner, E. P.; Lu, Y.; Liu, Y.; Zvyagin, A. V.; Zhang, L.; Dawes, J. M.; Xi, P.; Piper, J. A. *Nat. Nanotechnol.* **2013**, *8*, 729−734.

(25) Lu, Y.; Zhao, J.; Zhang, R.; Liu, Y.; Liu, D.; Goldys, E. M.; Yang, X.; Xi, P.; Sunna, A.; Lu, J. *Nat. Photonics* **2014**, *8*, 32−36.

(26) Lu, J.; Chen, Y.; Liu, D.; Ren, W.; Lu, Y.; Shi, Y.; Piper, J. A.; Paulsen, I. T.; Jin, D. *Anal. Chem.* **2015**, *87*, 10406.

(27) Min, Y.; Li, J.; Liu, F.; Padmanabhan, P.; Yeow, E. K.; Xing, B. *Nanomaterials* **2014**, *4*, 129−154.

(28) Zhou, J.; Sun, Y.; Du, X.; Xiong, L.; Hu, H.; Li, F. *Biomaterials* **2010**, *31*, 3287−3295.

(29) Liu, Q.; Feng, W.; Yang, T.; Yi, T.; Li, F. *Nat. Protoc.* **2013**, *8*, 2033−2044.

(30) Wang, F.; Banerjee, D.; Liu, Y.; Chen, X.; Liu, X. *Analyst* **2010**, *135*, 1839−1854.

(31) Zhou, J.; Liu, Q.; Feng, W.; Sun, Y.; Li, F. *Chem. Rev.* **2015**, *115*, 395−465.

(32) Nyk, M.; Kumar, R.; Ohulchanskyy, T. Y.; Bergey, E. J.; Prasad, P. N. *Nano Lett.* **2008**, *8*, 3834−3838.

(33) Chen, G.; Shen, J.; Ohulchanskyy, T. Y.; Patel, N. J.; Kutikov, A.; Li, Z.; Song, J.; Pandey, R. K.; Ågren, H.; Prasad, P. N.; Han, G. *ACS Nano* **2012**, *6*, 8280−8287.

(34) Dong, N.-N.; Pedroni, M.; Piccinelli, F.; Conti, G.; Sbarbati, A.; Ramírez-Hernández, J. E.; Maestro, L. M.; Iglesias-de la Cruz, M. C.; Sanz-Rodriguez, F.; Juarranz, A. *ACS Nano* **2011**, *5*, 8665−8671.

(35) Zheng, W.; Tu, D.; Huang, P.; Zhou, S.; Chen, Z.; Chen, X. *Chem. Commun.* **2015**, *51*, 4129−4143.

(36) Bünzli, J.-C. G. *Chem. Rev.* **2010**, *110*, 2729−2755.

(37) Yang, D.; Li, C.; Lin, J. *Nanomedicine* **2015**, *10*, 2573−2591.

(38) Naccache, R.; Rodríguez, E. M.; Bogdan, N.; Sanz-Rodríguez, F.; Cruz, M. d. C. I. d. l.; Fuente, Á. J. d. l.; Vetrone, F.; Jaque, D.; Solé, J. G.; Capobianco, J. A. *Cancers* **2012**, *4*, 1067−1105.

(39) Liu, Q.; Sun, Y.; Yang, T.; Feng, W.; Li, C.; Li, F. *J. Am. Chem. Soc.* **2011**, *133*, 17122−17125.

(40) Cheong, W.-F.; Prahl, S. A.; Welch, A. J. *IEEE J. Quantum Electron.* **1990**, *26*, 2166−2185.

DOI: 10.1021/acs.analchem.5b04626
Anal. Chem. XXXX, XXX, XXX−XXX

(41) del Rosal, B.; Villa, I.; Jaque, D.; Sanz-Rodríguez, F. *J. Biophotonics* **2015**, DOI: 10.1002/jbio.201500271.
(42) Khan, M. H.; Sink, R. K.; Manstein, D.; Eimerl, D.; Anderson, R. *Lasers Surg. Med.* **2005**, *36*, 270−280.
(43) Zhang, L.; Zheng, X.; Deng, W.; Lu, Y.; Lechevallier, S.; Ye, Z.; Goldys, E. M.; Dawes, J. M.; Piper, J. A.; Yuan, J. *Sci. Rep.* **2014**, *4*, 6597.
(44) Jin, D.; Piper, J. A. *Anal. Chem.* **2011**, *83*, 2294−2300.
(45) Song, B.; Ye, Z.; Yang, Y.; Ma, H.; Zheng, X.; Jin, D.; Yuan, J. *Sci. Rep.* **2015**, *5*, 14194.
(46) Pu, C.; Ma, J.; Qin, H.; Yan, M.; Fu, T.; Niu, Y.; Yang, X.; Huang, Y.; Zhao, F.; Peng, X. *ACS Cent. Sci.* **2016**, *2*, 32.
(47) Xie, X.; Gao, N.; Deng, R.; Sun, Q.; Xu, Q.-H.; Liu, X. *J. Am. Chem. Soc.* **2013**, *135*, 12608−12611.
(48) Shen, J.; Chen, G.; Vu, A. M.; Fan, W.; Bilsel, O. S.; Chang, C. C.; Han, G. *Adv. Opt. Mater.* **2013**, *1*, 644−650.
(49) Wang, Y.-F.; Liu, G.-Y.; Sun, L.-D.; Xiao, J.-W.; Zhou, J.-C.; Yan, C.-H. *ACS Nano* **2013**, *7*, 7200−7206.

DOI: 10.1021/acs.analchem.5b04626
Anal. Chem. XXXX, XXX, XXX−XXX